

Next-to-leading order QCD corrections to tZ associated production via the flavor-changing neutral-current couplings at hadron colliders

Bo Hua Li, Yue Zhang, Chong Sheng Li,^{*} Jun Gao, and Hua Xing Zhu

*Department of Physics and State Key Laboratory of Nuclear Physics and Technology,
Peking University, Beijing 100871, China*

(Dated: February 5, 2022)

Abstract

We present the complete next-to-leading order (NLO) QCD corrections to tZ associated production induced by the model-independent tqg and tqZ flavor-changing neutral-current couplings at hadron colliders, respectively. Our results show that, for the tuZ coupling the NLO QCD corrections can enhance the total cross sections by about 60% and 42%, and for the tcZ coupling by about 51% and 43% at the Tevatron and LHC, respectively. The NLO corrections, for the tug couplings, can enhance the total cross sections by about 27%, and by about 42% for the tcg coupling at the LHC. We also consider the mixing effects between the tqg and tqZ couplings for this process, which can either be large or small depending on the values of the anomalous couplings. Besides, the NLO corrections reduce the dependence of the total cross sections on the renormalization or factorization scale significantly, which lead to increased confidence on the theoretical predictions. And we also evaluate the NLO corrections to several important kinematic distributions.

PACS numbers: 14.65.Ha, 12.38.Bx, 12.60.Cn

^{*}Electronic address: csli@pku.edu.cn

I. INTRODUCTION

The mass of the top quark is close to the electroweak(EW) symmetry breaking scale, and thus its decay and production at colliders are very important for the probe of the EW breaking mechanism and new physics beyond the standard model (SM). Direct evidence of new physics at TeV scale may be not easy to find, while indirect evidence, such as modification of SM predictions originated from new physics interaction, is important as well. A good consideration is to investigate the single top quark production process via the anomalous flavor-changing neutral-current (FCNC) couplings. Within the SM, the FCNC couplings can only occur at the loop level, which are further suppressed by the GIM mechanism [1]. On the other hand, some new physics models [2, 3] such as the two Higgs doublet models [4], supersymmetric models [5], extra dimensions models [6], may enhance these FCNC couplings to observable level. As the coming Large Hadron Collider (LHC) will produce abundant top quark events (about 10^8 per year), even in the initial low luminosity run ($\sim 10 \text{ fb}^{-1}/\text{year}$) 8×10^6 top quark pairs and 3×10^6 single top quarks will be produced yearly, one may anticipate the discovery of the first hint of new physics by observing the FCNC couplings in the top quark sector.

In general, any new physics at a high energy scale Λ can be described by an effective Lagrangian containing higher dimensional SM gauge invariant operators [7]. For the new physics induced top-quark FCNC couplings related to the gluon and Z boson, respectively, they can be incorporated into the dimension five effective operators as listed below [8],

$$-g_s \sum_{q=u,c} \frac{\kappa_{tq}^g}{\Lambda} \bar{q} \sigma^{\mu\nu} T^a (f_{tq}^g + i h_{tq}^g \gamma_5) t G_{\mu\nu}^a - \frac{e}{\sin 2\theta_W} \sum_{q=u,c} \frac{\kappa_{tq}^Z}{\Lambda} \bar{q} \sigma^{\mu\nu} (f_{tq}^Z + i h_{tq}^Z \gamma_5) t Z_{\mu\nu} + H.c., \quad (1)$$

where Λ is the new physics scale, T^a are the Gell-Mann matrices, $G_{\mu\nu}^a$ and $Z_{\mu\nu}$ are the field strength tensors of the gluon and Z boson, respectively, κ_{tq}^Z ($q = u, c$) and κ_{tq}^g ($q = u, c$) are real coefficients that define the strength of the couplings. And θ_W is the weak-mixing angle, while f_{tq}^V and h_{tq}^V are complex numbers satisfying $|f_{tq}^V|^2 + |h_{tq}^V|^2 = 1$ with $V = Z, g$ and $q = u, c$.

The CDF collaboration has set 95% confidence level (CL) limits on the branching ratio $BR(t \rightarrow qZ) < 0.037$ [9], which corresponds to $\kappa_{tq}^Z/\Lambda < 0.908 \text{ TeV}^{-1}$ based on the theoretical predictions of $t \rightarrow qZ$ at the NLO level in QCD [10–13]. The D0 collaboration also provides a more stringent constrains, $BR(t \rightarrow qZ) < 0.032$ at a 95% confidence level [14], which

corresponds to $\kappa_{tq}^Z/\Lambda < 0.845\text{TeV}^{-1}$. Currently the most stringent experimental constraints for the tqg anomalous couplings are $\kappa_{tu}^g/\Lambda \leq 0.013\text{ TeV}^{-1}$ and $\kappa_{tc}^g/\Lambda \leq 0.057\text{ TeV}^{-1}$, given by the D0 collaboration [15], and $\kappa_{tu}^g/\Lambda \leq 0.018\text{ TeV}^{-1}$ and $\kappa_{tc}^g/\Lambda \leq 0.069\text{ TeV}^{-1}$ given by the CDF collaboration [16], both based on the measurements of the FCNC single top production using the theoretical predictions, including the NLO QCD corrections [17, 18] and resummation effects [19], respectively.

Since the observation of $pp \rightarrow tZ$ is a clear signal of top flavor violation, and we do not know which type of new physics will be responsible for a future deviation from the SM predictions, it is necessary to study this process in a model-independent way. There are already several literatures [20, 21] discussing this process using the effective Lagrangian in Eq. (1). However, they were either based on the LO calculations [20], or the NLO QCD effects are not completely calculated [21]. So it is necessary to present a complete NLO QCD corrections to the above process, which is not only mandatory for matching the expected experimental accuracy at hadron colliders, but is also important for a consistent treatment of both the top quark production and decay via the FCNC couplings by experiments. In this paper, we present the complete NLO QCD corrections to tZ associated production via tqZ and tqg FCNC couplings with their mixing effects at hadron colliders.

The arrangement of this paper is as follows. In Sec. II we show the LO results for the process induced by tqZ FCNC couplings. In Sec. III, we present the details of the NLO calculations, including the virtual and real corrections. We discuss the process induced by tqg FCNC couplings and the mixing effects in Sec. IV, Sec. V contains the numerical results, and Section VI is a brief summary.

II. LEADING ORDER RESULTS

At hadron colliders, there is only one subprocess that contributes to the tZ associated production at the LO via the electroweak FCNC couplings, κ_{tq}^Z :

$$g\ q \longrightarrow t\ Z, \quad (2)$$

where q is either u quark or c quark. The corresponding Feynman diagrams are shown in Fig. 1.

After sum over the spins and colors of the outgoing particles and average over the spins

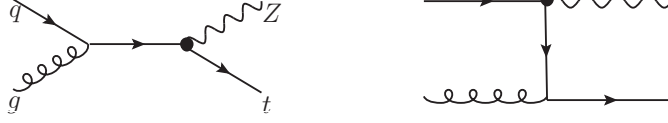


FIG. 1: The LO Feynman diagrams for the single top quark production via the FCNC couplings without operator mixing.

and colors of the incoming particles, the LO squared amplitude is

$$\begin{aligned} \overline{|M^B|^2}_{gq}(s, t) = & \frac{32\pi^2\alpha\alpha_s\kappa_z^2}{3\sin(2\theta_W)^2\Lambda^2s(t-m_t^2)^2}(2m_t^8 - (3m_z^2 + 4s + 2t)m_t^6 + \\ & (2m_z^4 - (2s + t)m_z^2 + 2(s^2 + 4ts + t^2))m_t^4 + (2m_z^6 - 4tm_z^4 \\ & + (s^2 + 6ts + 5t^2)m_z^2 - 2t(3s^2 + 6ts + t^2))m_t^2 + t(-2m_z^6 + 2 \\ & (s + t)m_z^4 - (s + t)^2m_z^2 + 4st(s + t))), \end{aligned} \quad (3)$$

where m_t is the top quark mass, and m_z is the Z boson mass, s , t , and u are the Mandelstam variables, which are defined as

$$s = (p_1 + p_2)^2, \quad t = (p_1 - p_3)^2, \quad u = (p_1 - p_4)^2. \quad (4)$$

After the phase space integration, the LO partonic cross sections are given by

$$\hat{\sigma}_{ab}^B = \frac{1}{2\hat{s}} \int d\Gamma \overline{|M^B|^2}_{ab}. \quad (5)$$

The LO total cross section at hadron colliders is obtained by convoluting the partonic cross section with the parton distribution functions (PDFs) $G_{i/P}$ for the proton (antiproton)

$$\sigma^B = \sum_{ab} \int dx_1 dx_2 [G_{a/P_1}(x_1, \mu_f) G_{b/P_2}(x_2, \mu_f) \hat{\sigma}_{ab}^B], \quad (6)$$

where μ_f is the factorization scale.

III. NEXT-TO-LEADING ORDER QCD CORRECTIONS

In this section, we present our calculations for the NLO QCD corrections to the tZ associated production via the electroweak FCNC couplings. The NLO corrections include both the virtual and the real corrections with the Feynman diagrams shown in Figs. 2-3, which are generated with FeynArts [22], and calculated with FormCalc [23]. We use the dimensional

regularization (DREG) scheme [24] with naive γ_5 prescription in $n = 4 - 2\epsilon$ dimensions to regularize all the divergences. Moreover, for the real corrections, we use the two-cutoff phase space slicing method [25] to separate the infrared(IR) divergences.

A. Virtual corrections

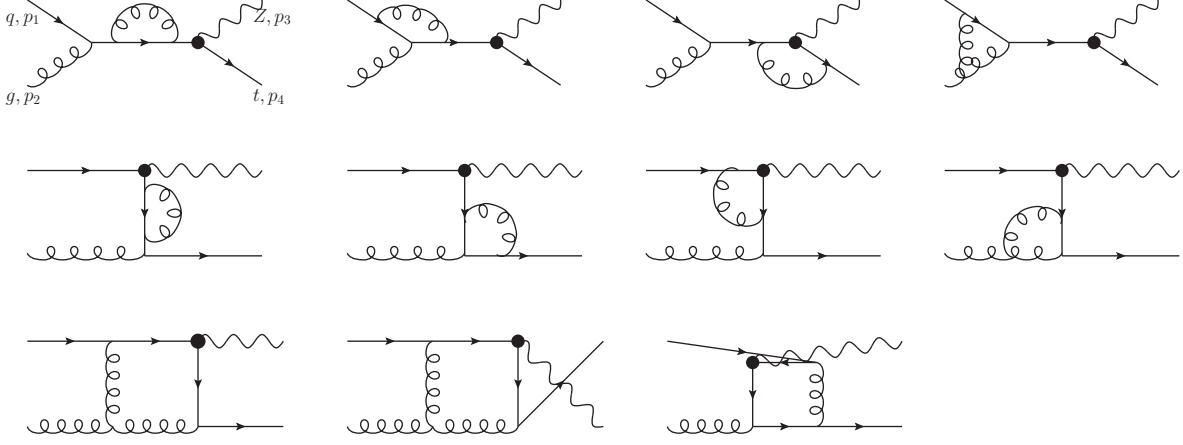


FIG. 2: 1-loop Feynman diagrams for the single top quark production via the FCNC couplings without operator mixing.

The virtual corrections contains both UV and IR divergences, with the UV divergences renormalized by introducing counterterms. For the external fields, we define all the renormalization constants using the on-shell subtraction scheme

$$\begin{aligned}
\delta Z_2^{(g)} &= -\frac{\alpha_s}{2\pi} C_\epsilon \left(\frac{n_f}{3} - \frac{5}{2} \right) \left(\frac{1}{\epsilon_{UV}} - \frac{1}{\epsilon_{IR}} \right) - \frac{\alpha_s}{6\pi} C_\epsilon \frac{1}{\epsilon_{UV}}, \\
\delta Z_2^{(q)} &= -\frac{\alpha_s}{3\pi} C_\epsilon \left(\frac{1}{\epsilon_{UV}} - \frac{1}{\epsilon_{IR}} \right), \\
\delta Z_2^{(t)} &= -\frac{\alpha_s}{3\pi} C_\epsilon \left(\frac{1}{\epsilon_{UV}} + \frac{2}{\epsilon_{IR}} + 4 \right), \\
\frac{\delta m_t}{m_t} &= -\frac{\alpha_s}{3\pi} C_\epsilon \left(\frac{3}{\epsilon_{UV}} + 4 \right),
\end{aligned} \tag{7}$$

where $C_\epsilon = \Gamma(1+\epsilon)[(4\pi\mu_r^2)/m_t^2]^\epsilon$ and $n_f = 5$. For the renormalization of the strong coupling constant g_s , and the FCNC couplings $\delta Z_{\kappa_{tq}^g/\Lambda}$, we use the $\overline{\text{MS}}$ scheme [10]:

$$\begin{aligned}\delta Z_{g_s} &= \frac{\alpha_s}{4\pi}\Gamma(1+\epsilon)(4\pi)^\epsilon \left(\frac{n_f}{3} - \frac{11}{2}\right) \frac{1}{\epsilon_{UV}} + \frac{\alpha_s}{12\pi}C_\epsilon \frac{1}{\epsilon_{UV}}, \\ \delta Z_{\kappa_{tq}^Z/\Lambda} &= \frac{\alpha_s}{3\pi}\Gamma(1+\epsilon)(4\pi)^\epsilon \frac{1}{\epsilon_{UV}},\end{aligned}\tag{8}$$

and the running of the FCNC couplings are given by [10]

$$\frac{\kappa_{tq}^Z(\mu)}{\Lambda} = \frac{\kappa_{tq}^Z(\mu')}{\Lambda} \left(\frac{\alpha_s(\mu')}{\alpha_s(\mu)}\right)^{4/(3\beta_0)},\tag{9}$$

with $\beta_0 = 11 - 2n_f/3$.

All the UV divergences cancel each other, leaving the remaining IR divergences and the finite terms. Because of the limited space, we do not shown the lengthy explicit expressions of the virtual corrections here. The IR divergence of the virtual corrections to the partonic total cross section can be factorized as [26, 27]

$$\hat{\sigma}_{IR}^{Loop} = -\frac{\alpha_s}{6\pi}D_\epsilon \left\{ \frac{13}{\epsilon_{IR}^2} + \left(4\ln\left(\frac{s}{m_t^2}\right) + \ln\left(\frac{m_t^2 - u}{m_t^2}\right) - 9\ln\left(\frac{m_t^2 - t}{m_t^2}\right) + \frac{43}{2} \right) \frac{1}{\epsilon_{IR}} \right\} \hat{\sigma}^B, \tag{10}$$

where $D_\epsilon = [(4\pi\mu_r^2)/s]^\epsilon/\Gamma(1-\epsilon)$. In order to cancel these divergences, we need to extract the IR divergences in the real corrections, which will be shown in the following subsection.

B. Real corrections

The real corrections consist of the radiations of an additional gluon $g \ q \longrightarrow t \ Z \ g$, or massless quark(anti) in the final states, $g \ g \longrightarrow t \ \bar{q} \ Z$, $q \ q(\bar{q}, q') \longrightarrow t \ q(\bar{q}, q') \ Z$, $q' \bar{q}' \longrightarrow t \ \bar{q} \ Z$ as shown in Fig. 3. It should be noted that in our NLO calculations of the process induced by tqZ couplings, we did not include the contributions from the SM on-shell production of the top quark pair with subsequent rare decay of one top quark, $pp(\bar{p}) \rightarrow t\bar{t} \rightarrow t + \bar{q} + Z$, and also the corresponding interference terms, following the diagram removal scheme proposed in reference [28]. This procedure does violate the gauge invariance because certain diagrams are removed, but the influence to the numerical results is small as show in [28]. We have also crosschecked the numerical results by using another method preserving gauge invariance [29], where an invariant mass cut of the Z boson and light quark is adopted. And the results of the invariant mass cut method agree well with the ones of the diagram removal method if we require the invariant mass to be out of the range of $\pm 17\Gamma_t$ of the top quark mass, where Γ_t is the width of top quark.

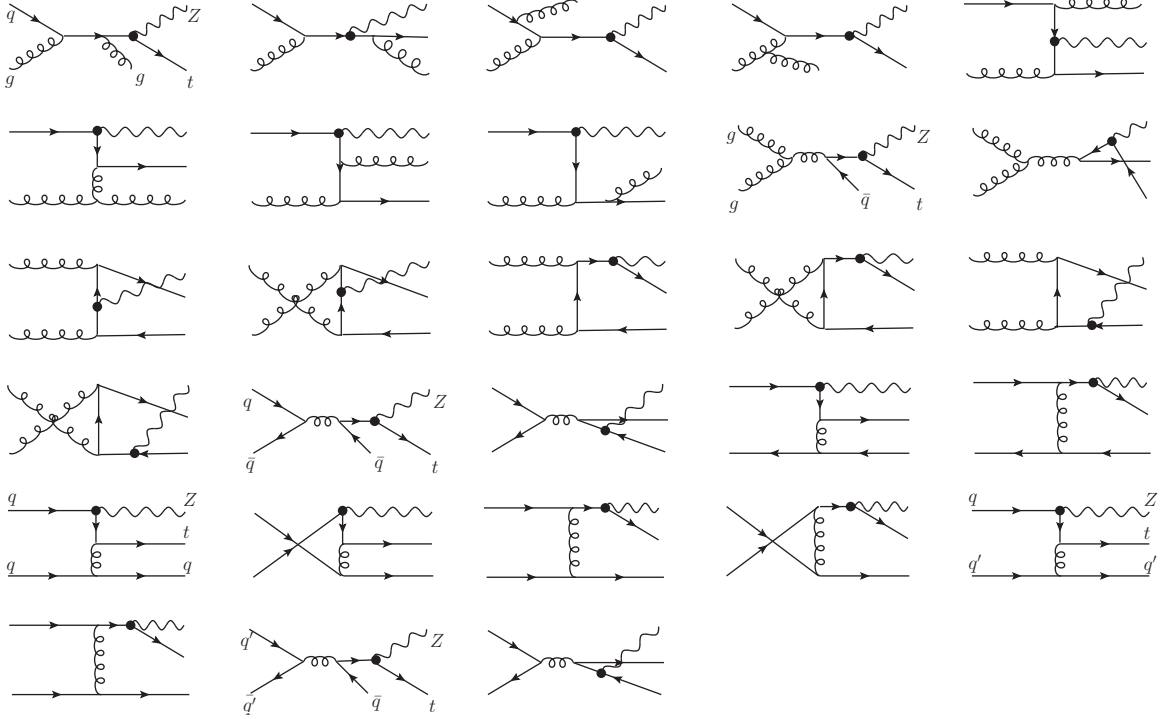


FIG. 3: Feynman diagrams of the real corrections for the single top quark production via the FCNC couplings without operator mixing.

1. Real gluon emission

For real gluon emission, the phase space integration contains both soft and collinear singularities. We adopt the two-cutoff phase space slicing method to isolate all the IR singularities [25], which introduces two small parameters δ_s and δ_c to divide the phase space into three parts. The soft cutoff δ_s separates the phase space into the soft region $E_5 \leq \delta_s \sqrt{s}/2$ and the hard region,

$$\hat{\sigma}^R = \hat{\sigma}^H + \hat{\sigma}^S, \quad (11)$$

furthermore, the hard piece can be divided into two sub-regions by δ_c ,

$$\hat{\sigma}^H = \hat{\sigma}^{\overline{\text{HC}}} + \hat{\sigma}^{\text{HC}}. \quad (12)$$

The hard noncollinear part $\hat{\sigma}^{\overline{\text{HC}}}$ is finite and the phase space integration can be calculated numerically. For the soft region, in the limit that the energy of the emitted gluon becomes

small, i.e. $E_5 \leq \delta_s \sqrt{s}/2$, the amplitude squared $\overline{\sum} |M(qg \rightarrow tZ + g)|^2$ can be factorized into the Born amplitude squared times an eikonal factor Φ_{eik}

$$\overline{\sum} |M(qg \rightarrow tZ + g)|^2 \xrightarrow{\text{soft}} (4\pi\alpha_s\mu_r^{2\epsilon}) \overline{\sum} |M^B|^2 \Phi_{\text{eik}}, \quad (13)$$

where the eikonal factor is given by

$$\begin{aligned} \Phi_{\text{eik}} = & \frac{C_A}{2} \frac{s}{(p_1 \cdot p_5)(p_2 \cdot p_5)} - \frac{1}{2C_A} \frac{m_t^2 - u}{(p_1 \cdot p_5)(p_4 \cdot p_5)} \\ & + \frac{C_A}{2} \frac{m_t^2 - t}{(p_2 \cdot p_5)(p_4 \cdot p_5)} - C_F \frac{m_t^2}{(p_4 \cdot p_5)^2}, \end{aligned} \quad (14)$$

where $C_A = 3, C_F = \frac{4}{3}$. Moreover, the three-body phase space in the soft limit can also be factorized

$$d\Gamma_3(qg \rightarrow tZ + g) \xrightarrow{\text{soft}} d\Gamma_2(qg \rightarrow tZ) dS. \quad (15)$$

Here dS is the integration over the phase space of the soft gluon which is given by[25]

$$dS = \frac{1}{2(2\pi)^{3-2\epsilon}} \int_0^{\delta_s \sqrt{s}/2} dE_5 E_5^{1-2\epsilon} d\Omega_{2-2\epsilon}. \quad (16)$$

The parton level cross section in the soft region can be expressed as

$$\hat{\sigma}^S = (4\pi\alpha_s\mu_r^{2\epsilon}) \int d\Gamma_2 \overline{\sum} |M^B|^2 \int dS \Phi_{\text{eik}}. \quad (17)$$

After the integration over the soft gluon phase space[25], Eq.(17) becomes

$$\hat{\sigma}^S = \hat{\sigma}^B \left[\frac{\alpha_s}{2\pi} \frac{\Gamma(1-\epsilon)}{\Gamma(1-2\epsilon)} \left(\frac{4\pi\mu_r^2}{s} \right)^\epsilon \right] \left(\frac{A_2^s}{\epsilon^2} + \frac{A_1^s}{\epsilon} + A_0^s \right), \quad (18)$$

with

$$\begin{aligned} A_2^s &= \frac{13}{6\pi}, \\ A_1^s &= \frac{1}{6\pi} \left\{ -26\ln(\delta_s) + 4\ln\left(\frac{s}{m_t^2}\right) - \ln\left(\frac{m_t^2}{m_t^2 - u}\right) + 9\ln\left(\frac{m_t^2}{m_t^2 - t}\right) + 4 \right\}, \\ A_0^s &= \frac{1}{12\pi} \left\{ 52\ln^2(\delta_s) - 2 \left[\ln\left(\frac{(m_t^2 - t)^2}{sm_t^2}\right) - 9\ln\left(\frac{(-m_z^2 + s + t)^2}{sm_t^2}\right) + 8 \right] \ln(\delta_s) \right. \\ &\quad \left. + A + 9B_- - B_+ \right\}, \end{aligned} \quad (19)$$

where A and B_\pm , are given in Appendix.

In the hard collinear region, $E_5 > \delta_s \sqrt{s}/2$ and $-\delta_c s < t_{i5} < 0$, the emitted hard gluon is collinear to one of the incoming partons. As a consequence of the factorization theorem[30, 31] the matrix element squared for $qg \rightarrow tZ + g$ can be factorized into the product of the Born amplitude squared and the Altarelli-Parisi splitting function

$$\overline{\sum} |M(qg \rightarrow tZ + g)|^2 \xrightarrow{\text{collinear}} (4\pi\alpha_s\mu_r^{2\epsilon}) \overline{\sum} |M^B|^2 \left(\frac{-2P_{qq}(z, \epsilon)}{zt_{15}} + \frac{-2P_{gg}(z, \epsilon)}{zt_{25}} \right), \quad (20)$$

where z denotes the fraction of the momentum of the incoming parton carried by $q(g)$ with the emitted gluon taking a fraction $(1 - z)$, and the unregulated Altarelli-Parisi splitting functions are written explicitly as [25]

$$\begin{aligned} P_{qq}(z, \epsilon) &= C_F \left(\frac{1+z^2}{1-z} - \epsilon(1-z) \right), \\ P_{gg}(z, \epsilon) &= 2N \left(\frac{z}{1-z} + \frac{1-z}{z} + z(1-z) \right). \end{aligned} \quad (21)$$

Moreover, the three-body phase space can also be factorized in the collinear limit, for example, in the limit $-\delta_c s < t_{15} < 0$ it has the following form[25]

$$d\Gamma_3(qg \rightarrow tZ + g) \xrightarrow{\text{collinear}} d\Gamma_2(qg \rightarrow tZ; s' = zs) \frac{(4\pi)^\epsilon}{16\pi^2\Gamma(1-\epsilon)} dz dt_{15} [-(1-z)t_{15}]^{-\epsilon}. \quad (22)$$

Thus, after convoluting with the PDFs, the three-body cross section in the hard collinear region is given by[25]

$$\begin{aligned} d\sigma^{HC} &= d\hat{\sigma}^B \left[\frac{\alpha_s}{2\pi} \frac{\Gamma(1-\epsilon)}{\Gamma(1-2\epsilon)} \left(\frac{4\pi\mu_r^2}{s} \right)^\epsilon \right] \left(-\frac{1}{\epsilon} \right) \delta_c^{-\epsilon} \left[P_{qq}(z, \epsilon) G_{q/p}(x_1/z) G_{g/p}(x_2) \right. \\ &\quad \left. + P_{gg}(z, \epsilon) G_{g/p}(x_1/z) G_{q/p}(x_2) + (x_1 \leftrightarrow x_2) \right] \frac{dz}{z} \left(\frac{1-z}{z} \right)^{-\epsilon} dx_1 dx_2. \end{aligned} \quad (23)$$

where $G_{q(g)/p}(x)$ is the bare PDF.

2. Massless (anti)quark emission

In addition to the real gluon emission, a second set of real emission corrections to the inclusive cross section for $pp \rightarrow tZ$ at NLO involves the processes with an additional massless $q(\bar{q})$ in the final state. Since the contributions from real massless $q(\bar{q})$ emission contain initial state collinear singularities we need to use the two cutoff phase space slicing method [25] to isolate these collinear divergences. The cross sections for the processes with an additional

massless $q(\bar{q})$ in the final state can be expressed as

$$\begin{aligned}
d\sigma^{add} = & \sum_{(\alpha=q,\bar{q},q')} \left\{ \hat{\sigma}^{\overline{C}}(q\alpha \rightarrow tZ + q(\bar{q})) G_{q/p}(x_1) G_{\alpha/p}(x_2) + \right. \\
& d\hat{\sigma}^B \left[\frac{\alpha_s}{2\pi} \frac{\Gamma(1-\epsilon)}{\Gamma(1-2\epsilon)} \left(\frac{4\pi\mu_r^2}{s} \right)^\epsilon \right] \left(-\frac{1}{\epsilon} \right) \delta_c^{-\epsilon} P_{g\alpha}(z, \epsilon) G_{q/p}(x_1/z) G_{\alpha/p}(x_2) \\
& \frac{dz}{z} \left(\frac{1-z}{z} \right)^{-\epsilon} + (x_1 \leftrightarrow x_2) \Big\} dx_1 dx_2 + \left\{ \hat{\sigma}^{\overline{C}}(gg \rightarrow tZ + \bar{q}) G_{g/p}(x_1) G_{g/p}(x_2) + \right. \\
& d\hat{\sigma}^B \left[\frac{\alpha_s}{2\pi} \frac{\Gamma(1-\epsilon)}{\Gamma(1-2\epsilon)} \left(\frac{4\pi\mu_r^2}{s} \right)^\epsilon \right] \left(-\frac{1}{\epsilon} \right) \delta_c^{-\epsilon} P_{gq}(z, \epsilon) G_{g/p}(x_1/z) G_{g/p}(x_2) \\
& \left. \frac{dz}{z} \left(\frac{1-z}{z} \right)^{-\epsilon} + (x_1 \leftrightarrow x_2) \Big\} dx_1 dx_2, \tag{24}
\end{aligned}$$

where

$$\begin{aligned}
P_{qg}(z, \epsilon) &= P_{\bar{q}g}(z) = \frac{1}{2} [z^2 + (1-z)^2] - z(1-z)\epsilon, \\
P_{gq}(z, \epsilon) &= P_{g\bar{q}}(z) = C_F \left[\frac{z}{1+(1-z)^2} - z\epsilon \right]. \tag{25}
\end{aligned}$$

The $\hat{\sigma}^{\overline{C}}$ terms in Eq. (24) represents the noncollinear cross sections for the $q(\bar{q}, q, q')$ and gg initiated processes which can be written in the form

$$\hat{\sigma}^C = \frac{1}{2s} \left\{ \sum_{(\alpha=q,\bar{q},q')} |M(q(\bar{q}, q, q')) \xrightarrow{\text{collinear}} tZ + (\bar{q}, q, q')|^2 + |M(gg) \xrightarrow{\text{collinear}} tZ + \bar{q})|^2 \right\} d\bar{\Gamma}_3, \tag{26}$$

where $d\bar{\Gamma}_3$ is the three-body phase space in the noncollinear region. The other terms in Eq. (24) are the collinear singular cross sections.

3. Mass factorization

After adding the renormalized virtual corrections and the real corrections, the parton level cross sections still contain collinear divergences which can be absorbed into a redefinition of the PDFs at the NLO, namely through mass factorization[32, 33]. This procedure, in practice, means that first we convolute the partonic cross section with the bare PDF $G_{\alpha/p}(x)$ and then use the renormalized PDF $G_{\alpha/p}(x, \mu_f)$ to replace $G_{\alpha/p}(x)$. In the $\overline{\text{MS}}$ convention

the scale-dependent PDF $G_{\alpha/p}(x, \mu_f)$ is given by [25]

$$G_{\alpha/p}(x, \mu_f) = G_{\alpha/p}(x) + \sum_{\beta} \left(-\frac{1}{\epsilon} \right) \left[\frac{\alpha_s}{2\pi} \frac{\Gamma(1-\epsilon)}{\Gamma(1-2\epsilon)} \times \left(\frac{4\pi\mu_r^2}{\mu_f^2} \right)^\epsilon \right] \\ \times \int_x^1 \frac{dz}{z} P_{\alpha\beta}(z) G_{\beta/p}(x/z). \quad (27)$$

Then the $\mathcal{O}(\alpha_s)$ expression for the remaining collinear contribution can be written in the following form:

$$d\sigma^{coll} = d\hat{\sigma}^B \left[\frac{\alpha_s}{2\pi} \frac{\Gamma(1-\epsilon)}{\Gamma(1-2\epsilon)} \left(\frac{4\pi\mu_r^2}{s} \right)^\epsilon \right] \{ \tilde{G}_{q/p}(x_1, \mu_f) G_{g/p}(x_2, \mu_f) + G_{q/p}(x_1, \mu_f) \tilde{G}_{g/p}(x_2, \mu_f) \\ + \sum_{\alpha=q,g} \left[\frac{A_1^{sc}(\alpha \rightarrow \alpha g)}{\epsilon} + A_0^{sc}(\alpha \rightarrow \alpha g) \right] G_{q/p}(x_1, \mu_f) G_{\bar{q}/p}(x_2, \mu_f) \\ + (x_1 \leftrightarrow x_2) \} dx_1 dx_2, \quad (28)$$

where

$$A_0^{sc} = A_1^{sc} \ln\left(\frac{s}{\mu_f^2}\right), \quad (29)$$

$$A_1^{sc}(q \rightarrow qg) = C_F(2 \ln \delta_s + 3/2), \quad (30)$$

$$A_1^{sc}(g \rightarrow gg) = 2N \ln \delta_s + (11N - 2n_f)/6, \quad (31)$$

$$\tilde{G}_{\alpha/p}(x, \mu_f) = \sum_{\beta, \alpha} \int_x^{1-\delta_s \delta_{\alpha\beta}} \frac{dy}{y} G_{\beta/p}(x/y, \mu_f) \tilde{P}_{\alpha\beta}(y), \quad (32)$$

with

$$\tilde{P}_{\alpha\beta}(y) = P_{\alpha\beta}(y) \ln(\delta_c \frac{1-y}{y} \frac{s}{\mu_f^2}) - P'_{\alpha\beta}(y), \quad (33)$$

where $N = 3, n_f = 5$.

Putting together all pieces of the real correction, we can see that the IR divergences from the real correction can be written as

$$\sigma_{IR}^{Real} = \frac{\alpha_s}{6\pi} D_\epsilon \left\{ \frac{13}{\epsilon_{IR}^2} + \left(4 \ln\left(\frac{s}{m_t^2}\right) + \ln\left(\frac{m_t^2 - u}{m_t^2}\right) - 9 \ln\left(\frac{m_t^2 - t}{m_t^2}\right) + \frac{43}{2} \right) \frac{1}{\epsilon_{IR}} \right\} \sigma^B, \quad (34)$$

and all the IR divergences from the virtual corrections in Eq. (10) are canceled exactly, as we expected.

IV. CONTRIBUTIONS FROM THE ELECTROWEAK AND STRONG FCNC COUPLINGS AND THE MIXING EFFECTS

In previous sections, we only consider the contributions from the electroweak FCNC couplings, κ_{tq}^Z . However, for the tZ associated production process, there are additional contributions from the strong FCNC couplings, κ_{tq}^g , and the mixing effects between these two couplings. Since the magnitudes of the coefficients $\kappa_{tq}^V (V = Z, g)$ depend on the underlying new physics, the mixing effects may be significant in certain model. The $O(\alpha_s)$ corrections to the process $pp \rightarrow tZ$ induced by tqg are similar to ones induced by tqZ , so we don't show its analytical results, and only present the mixing effects in this section.

At the LO, the contributing Feynman diagrams are show in Fig. 4, and the squared amplitudes are present in the Appendix. The NLO corrections, which include the loop diagrams and the real emission diagrams, are shown in Fig. 12 and Fig. 13.

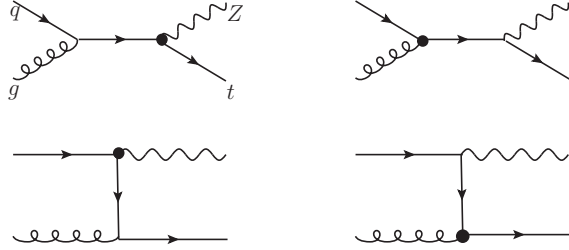


FIG. 4: The LO Feynman diagrams for the single top quark production via the FCNC couplings with operator mixing.

The relevant renormalization constants are the same as ones in Eq. (7) and (8), except that we introduce additional renormalization constants. We adopt the definition in Ref. [11]

$$\mathcal{L}_{\text{eff}} + \delta\mathcal{L}_{\text{eff}} = \begin{pmatrix} -\kappa^g & -\kappa^Z \end{pmatrix} \begin{pmatrix} 1 + \delta Z_{gg} & \delta Z_{gZ} \\ \delta Z_{Zg} & 1 + \delta Z_{ZZ} \end{pmatrix} \begin{pmatrix} O_g \\ O_Z \end{pmatrix}, \quad (35)$$

where the operators O_i ($i = g, Z$) are defined as $O_g = g_s \bar{q} \sigma^{\mu\nu} T^a (f_{tq}^g + i h_{tq}^g \gamma_5) t G_{\mu\nu}^a$, $O_Z = \frac{e}{\sin 2\theta_W} \bar{q} \sigma^{\mu\nu} (f_{tq}^Z + i h_{tq}^Z \gamma_5) t Z_{\mu\nu}$, and $\delta Z_{gg} = \delta Z_{\kappa_{tq}^g/\Lambda}$, $\delta Z_{ZZ} = \delta Z_{\kappa_{tq}^Z/\Lambda}$. At the $\mathcal{O}(\alpha_s)$ level, $\delta Z_{\kappa_{tq}^Z/\Lambda}$ is presented in Eq. (8), and other renormalization constants are given by:

$$\begin{aligned}
\delta Z_{\kappa_{tq}^g/\Lambda} &= \frac{\alpha_s}{6\pi} \Gamma(1+\epsilon) (4\pi)^\epsilon \frac{1}{\epsilon_{UV}}, \\
\delta Z_{gZ} &= \frac{\alpha_s}{3\pi} \Gamma(1+\epsilon) (4\pi)^\epsilon \frac{c_1 + c_2}{\epsilon_{UV}}, \\
\delta Z_{Zg} &= 0,
\end{aligned} \tag{36}$$

δZ_{gZ} is defined at the level of the cross section, and c_1, c_2 are defined as follows:

$$\begin{aligned}
c_1 &= g_{ZL}^* g_{gL} Q_f \sin\theta_W - g_{ZR}^* g_{gR} \frac{s_3 - Q_f \sin^2\theta_W}{\sin\theta_W}, \\
c_2 &= g_{ZR}^* g_{gR} Q_f \sin\theta_W - g_{ZL}^* g_{gL} \frac{s_3 - Q_f \sin^2\theta_W}{\sin\theta_W},
\end{aligned}$$

where Q_f is the electric charge of the fermion, and s_3 is its third component of the $SU(2)_L$ gauge group.

The renormalization group running for κ^V are modified to [11]:

$$\begin{aligned}
\frac{\kappa_{tq}^g(\mu)}{\Lambda} &= \frac{\kappa_{tq}^g(\mu')}{\Lambda} \eta^{\frac{2}{3\beta_0}}, \\
\frac{\kappa_{tq}^Z(\mu)}{\Lambda} &= \frac{\kappa_{tq}^Z(\mu')}{\Lambda} \eta^{\frac{4}{3\beta_0}} + \frac{\kappa_{tq}^g(\mu')}{\Lambda} \left(\frac{32}{3} \sin^2\theta_W - 4 \right) \left(\eta^{\frac{4}{3\beta_0}} - \eta^{\frac{2}{3\beta_0}} \right),
\end{aligned} \tag{37}$$

where $\eta = \frac{\alpha_s(\mu')}{\alpha_s(\mu)}$.

The IR divergence appearing in the virtual corrections has the same form as given in section III, except using the LO amplitude including the contributions from both the electroweak and the strong FCNC couplings instead of $\hat{\sigma}^B$.

V. NUMERICAL RESULTS

A. Process via tqZ FCNC couplings without operator mixing effects

We first consider the tZ associated production via the tqZ FCNC couplings, including the NLO QCD effects on the total cross sections, the scale dependence, and several important distributions at both the Tevatron and LHC. All the SM input parameters are taken to be [34]:

$$m_t = 172.0 \text{ GeV}, \quad \alpha_s(M_Z) = 0.118, \quad \alpha = 1/128.921. \tag{38}$$

And we set the electroweak FCNC couplings, allowed by current experiment, as follows:

$$\kappa_{tu}^Z/\Lambda = \kappa_{tc}^Z/\Lambda = 0.5 \text{ TeV}^{-1}. \tag{39}$$

The running QCD coupling constant is evaluated at the three-loop order [35] and the CTEQ6M PDF set [36] is used throughout the calculations of the NLO (LO) cross sections. Both the renormalization and factorization scales are fixed to the sum of the top quark and the Z boson mass.

In Table I, we list some typical numerical results of the LO and NLO total cross sections for the tZ associated production via the electroweak FCNC couplings. It can be seen that, for the tuZ coupling the NLO corrections can enhance the total cross sections by about 60% and 42%, and for the tcZ coupling by about 51% and 43% at the Tevatron and LHC, respectively.

FCNC coupling	tuZ (LO)	tuZ (NLO)	tcZ (LO)	tcZ (NLO)
LHC (pb)	15.9	22.5	1.29	1.85
Tevatron (fb)	55.5	88.6	1.62	2.45

TABLE I: The LO and NLO total cross sections for tZ associated production via the electroweak FCNC couplings at both the LHC and Tevatron. Here $\mu = m_t + m_z$, $\kappa_{tq}^Z/\Lambda = 0.5\text{TeV}^{-1}$.

In Fig.5 we show that it is reasonable to use the two cutoff phase space slicing method in our NLO QCD calculations; i.e., the dependence of the NLO QCD predictions on the arbitrary cutoffs δ_s and δ_c is indeed very weak. While the Born cross sections and the virtual corrections are cutoff independent, both the soft and collinear contributions and the noncollinear contributions depend strongly on the cutoffs. However, the cutoff dependence in the two contributions ($\sigma^S + \sigma^{coll}$ and $\sigma^{\overline{HC}} + \sigma^{\overline{C}}$) nearly cancel each other, and the final results for σ^{NLO} are almost independent of the cutoffs. We will take $\delta_s = 10^{-4}$ in the numerical calculations below. Generally δ_c being 50 – 100 times smaller than δ_s is sufficient for accurate calculations to a few percent[25], so we take $\delta_c = \delta_s/50$ in our calculations.

In Figs. 6 we show the scale dependence of the LO and NLO total cross section for three cases: (1) the renormalization scale dependence $\mu_r = \mu$, $\mu_f = m_t + m_Z$; (2) the factorization scale dependence $\mu_r = m_t + m_Z$, $\mu_f = \mu$; and (3) total scale dependence $\mu_r = \mu_f = \mu$. It can be seen that the NLO corrections reduce the scale dependence for all three cases, which make the theoretical predictions more reliable. Fig. 7 give the p_T distributions of the top quark and the Z boson, respectively, and Fig 8 shows the invariant mass distributions of the Z boson and the top quark.

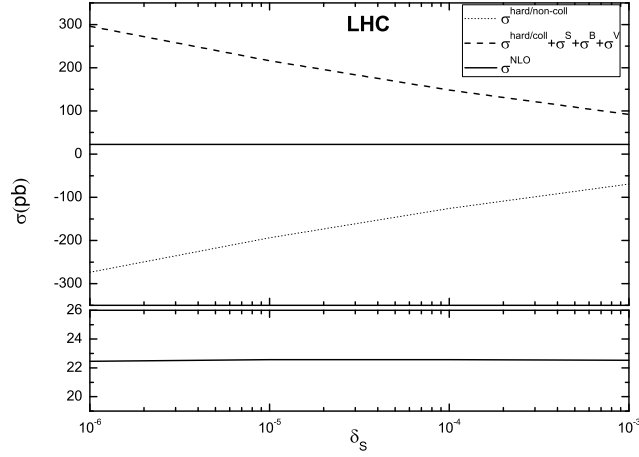


FIG. 5: Inclusive total cross sections for $pp \rightarrow tZ + X$ at the LHC as a function of δ_s in the phase space slicing treatment. The δ_c is chosen to be $\delta_c = \delta_s/50$.

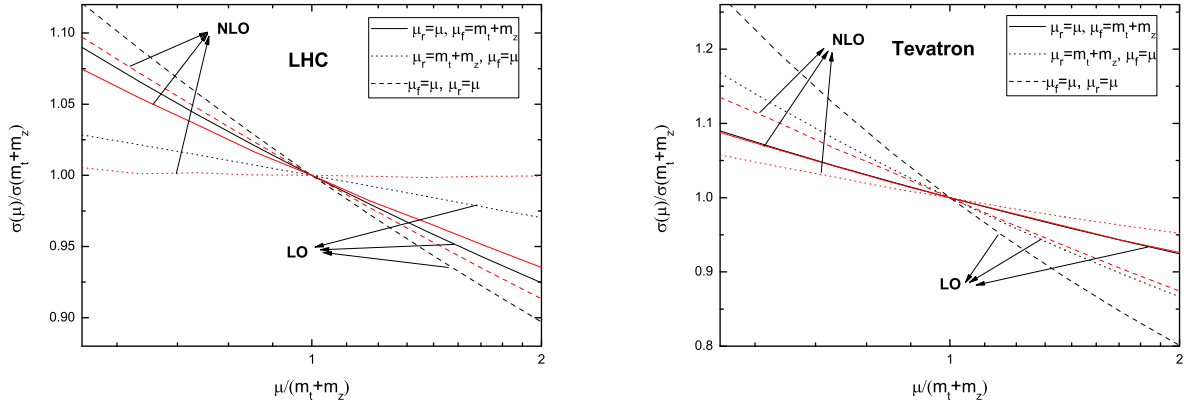


FIG. 6: Scale dependence of the total cross sections for the gu initial state subprocess at both LHC and Tevatron, the black lines represent the LO results, while the red ones represent the NLO results.

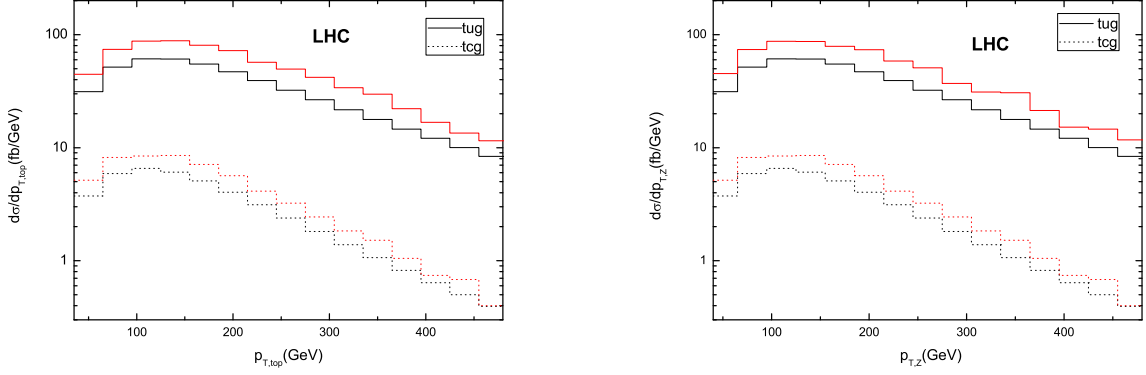


FIG. 7: p_T distributions of the top quark and the Z boson at LHC, the black and red lines represent the LO and the NLO results of the FCNC single top production, respectively.

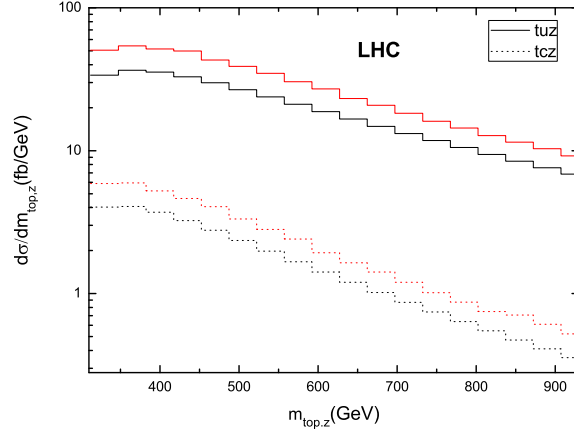


FIG. 8: Invariant mass distributions of the Z boson and the top quark, the black and red lines represent the LO and the NLO results of the FCNC single top production, respectively.

B. Process include operator mixing effects

In this subsection, we present the numerical results of the tZ associated production via the electroweak and strong FCNC couplings, including the NLO QCD effects and the mixing effects. We investigate the NLO QCD effects on the total cross sections and the scale dependence at the LHC. For the numerical calculations, we take the same SM parameters as above subsection.

In Table II, we list some typical numerical results of the LO and NLO total cross sections for the tZ associated production via the strong FCNC couplings, assuming $\kappa_{tq}^g/\Lambda = 0.01\text{TeV}^{-1}$, allowed by current experiment. It can be seen that, the NLO corrections can enhance the total cross sections by about 27% for the tug couplings, and by about 42% for the tcg coupling at the LHC. Nevertheless, the contributions to the total cross sections from the process induced by the tqZ FCNC couplings are still dominate.

FCNC coupling	tug (LO)	tug (NLO)	tcg (LO)	tcg (NLO)
LHC (fb)	141	180	7.6	10.8

TABLE II: The LO and the NLO total cross sections for the tZ associated production via the strong FCNC couplings at the LHC. Here $\mu = m_t + m_z$, $\kappa_{tq}^g/\Lambda = 0.01\text{TeV}^{-1}$, and $|g_{gL}|^2 = |g_{gR}|^2 = 1$.

After considering the mixing effects, the total cross sections of the tZ associated production via FCNC couplings can be factorized as:

$$\begin{aligned} \sigma = & A_1 |g_{gL}|^2 \left(\frac{\kappa_{tq}^g}{\Lambda}\right)^2 + A_2 |g_{gR}|^2 \left(\frac{\kappa_{tq}^g}{\Lambda}\right)^2 + A_3 \left(\frac{\kappa_{tq}^Z}{\Lambda}\right)^2 + \\ & [A_4 \text{Re}(g_{gL}g_{ZL}^*) - A_5 \text{Re}(g_{gR}g_{ZR}^*)] \frac{\kappa_{tq}^g \kappa_{tq}^Z}{\Lambda^2}, \end{aligned} \quad (40)$$

where A_i represent the contributions from different couplings and mixing effects. And, their

FCNC coupling	tuV (LO)	tuV (NLO)	tcV (LO)	tcV (NLO)
LHC (fb)	147	188	8.1	11.5

TABLE III: The LO and the NLO total cross sections for the tZ associated production via the FCNC couplings at the LHC. Here $\mu = m_t + m_z$, $\kappa_{tq}^V/\Lambda = 0.01\text{TeV}^{-1}$ and $|g_{gL}|^2 = |g_{gR}|^2 = \text{Re}(g_{gL}g_{ZL}^*) = \text{Re}(g_{gR}g_{ZR}^*) = 1$.

numerical expressions at the LHC can be written as

$$\begin{aligned} \sigma_{LO}^{tuV} = & \left\{ 715|g_{gL}|^2 \left(\frac{\kappa_{tu}^g}{\Lambda}\right)^2 + 699|g_{gR}|^2 \left(\frac{\kappa_{tu}^g}{\Lambda}\right)^2 + 63.7 \left(\frac{\kappa_{tu}^Z}{\Lambda}\right)^2 \right. \\ & \left. + [76.0 \text{Re}(g_{gL}g_{ZL}^*) - 84.1 \text{Re}(g_{gR}g_{ZR}^*)] \frac{\kappa_{tu}^g \kappa_{tu}^Z}{\Lambda^2} \right\} (\text{pb} \cdot \text{TeV}^2), \end{aligned} \quad (41)$$

$$\begin{aligned} \sigma_{NLO}^{tuV} = & \left\{ 925|g_{gL}|^2 \left(\frac{\kappa_{tu}^g}{\Lambda}\right)^2 + 874|g_{gR}|^2 \left(\frac{\kappa_{tu}^g}{\Lambda}\right)^2 + 90 \left(\frac{\kappa_{tu}^Z}{\Lambda}\right)^2 \right. \\ & \left. + [107 \text{Re}(g_{gL}g_{ZL}^*) - 114 \text{Re}(g_{gR}g_{ZR}^*)] \frac{\kappa_{tu}^g \kappa_{tu}^Z}{\Lambda^2} \right\} (\text{pb} \cdot \text{TeV}^2), \end{aligned} \quad (42)$$

$$\begin{aligned} \sigma_{LO}^{tcV} = & \left\{ 38.9|g_{gL}|^2 \left(\frac{\kappa_{tc}^g}{\Lambda}\right)^2 + 37.2|g_{gR}|^2 \left(\frac{\kappa_{tc}^g}{\Lambda}\right)^2 + 5.15 \left(\frac{\kappa_{tc}^Z}{\Lambda}\right)^2 \right. \\ & \left. + [6.97 \text{Re}(g_{gL}g_{ZL}^*) - 7.47 \text{Re}(g_{gR}g_{ZR}^*)] \frac{\kappa_{tc}^g \kappa_{tc}^Z}{\Lambda^2} \right\} (\text{pb} \cdot \text{TeV}^2), \end{aligned} \quad (43)$$

$$\begin{aligned} \sigma_{NLO}^{tcV} = & \left\{ 56.7|g_{gL}|^2 \left(\frac{\kappa_{tc}^g}{\Lambda}\right)^2 + 51.5|g_{gR}|^2 \left(\frac{\kappa_{tc}^g}{\Lambda}\right)^2 + 7.38 \left(\frac{\kappa_{tc}^Z}{\Lambda}\right)^2 \right. \\ & \left. + [9.13 \text{Re}(g_{gL}g_{ZL}^*) - 9.83 \text{Re}(g_{gR}g_{ZR}^*)] \frac{\kappa_{tc}^g \kappa_{tc}^Z}{\Lambda^2} \right\} (\text{pb} \cdot \text{TeV}^2), \end{aligned} \quad (44)$$

where g_{iL}, g_{iR} are chiral parameters:

$$g_{iL} = f_{tq}^i - i h_{tq}^i, \quad g_{iR} = f_{tq}^i + i h_{tq}^i, \quad |g_{iL}|^2 + |g_{iR}|^2 = 2.$$

In Table III, we list some typical numerical results of the LO and NLO total cross sections by choosing a special set of parameters (for simplicity, we set $\kappa_{tq}^Z/\Lambda = \kappa_{tq}^g/\Lambda = 0.01\text{TeV}^{-1}$) and fix $\mu = m_t + m_Z$. For the $g u \rightarrow t Z$, the NLO corrections can enhance the total cross sections by about 28%, and for the $g c \rightarrow t Z$ process, by about 42% at the LHC.

To investigate the contributions from the operator mixing effects, we present the counter curves for the variables $\kappa_Z/\Lambda, \kappa_g/\Lambda$, and $\text{Re}(g_{gL}^*g_{ZL}), \text{Re}(g_{gR}^*g_{ZR})$ in Figs. 9, 10

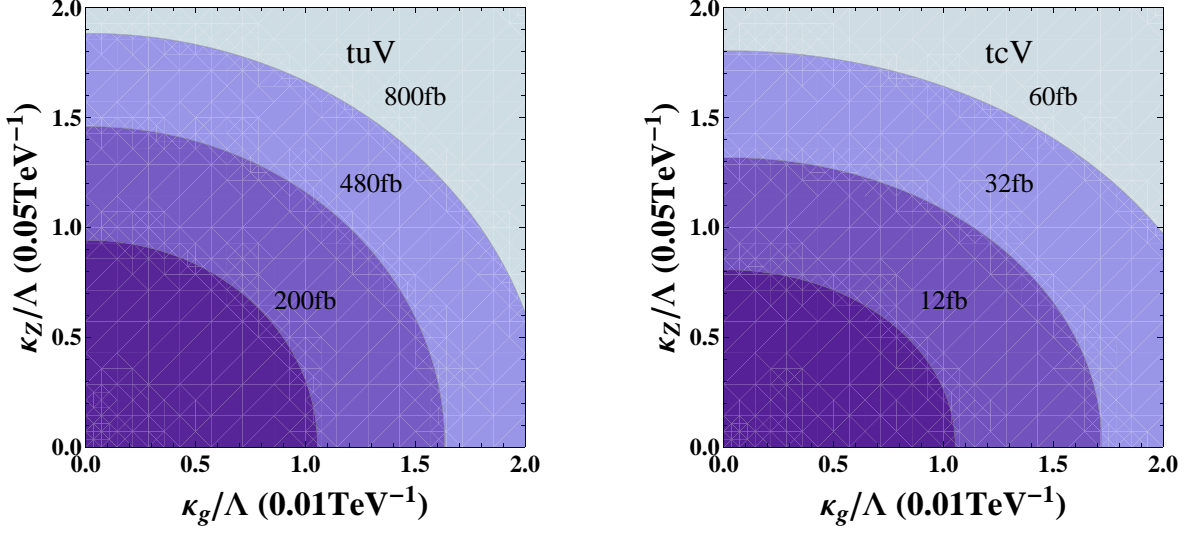


FIG. 9: The contour curves of the total cross sections versus the parameters κ_g/Λ and κ_z/Λ for the process induced by tuV and tcV FCNC couplings. Here we set $|g_{gL}|^2 = |g_{gR}|^2 = \text{Re}(g_{gL}g_{ZL}^*) = \text{Re}(g_{gR}g_{ZR}^*) = 1$.

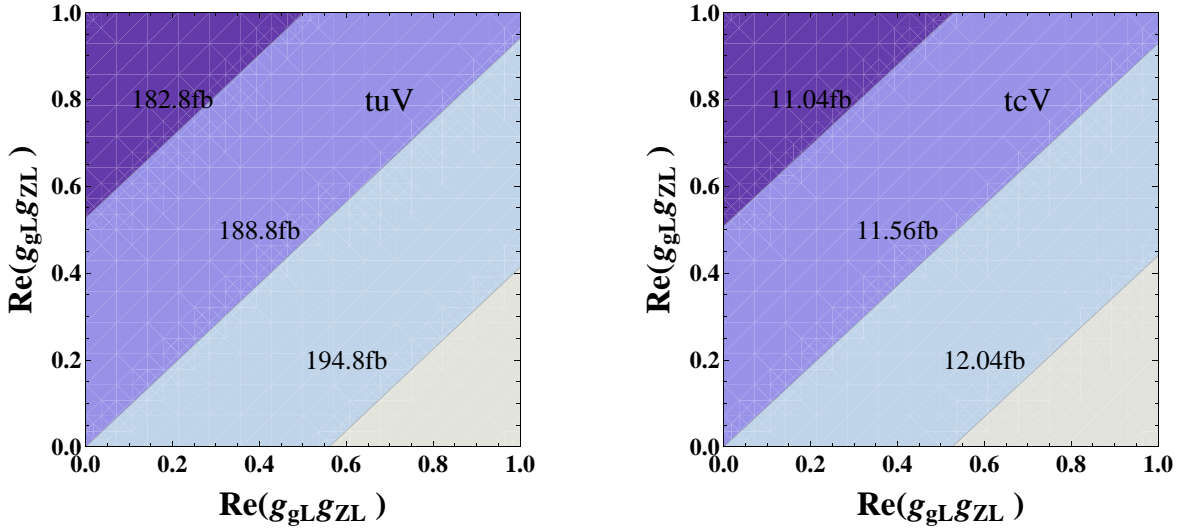


FIG. 10: The contour curves of the total cross sections versus the parameters $\text{Re}(g_{gL} \times g_{ZL})$ and $\text{Re}(g_{gR} \times g_{ZR})$ for the process induced by tuV and tcV FCNC couplings. Here we set $|g_{gL}|^2 = |g_{gR}|^2 = |g_{ZL}|^2 = |g_{ZR}|^2 = 1$ and $\kappa_g/\Lambda = \kappa_z/\Lambda = 0.01\text{TeV}^{-1}$.

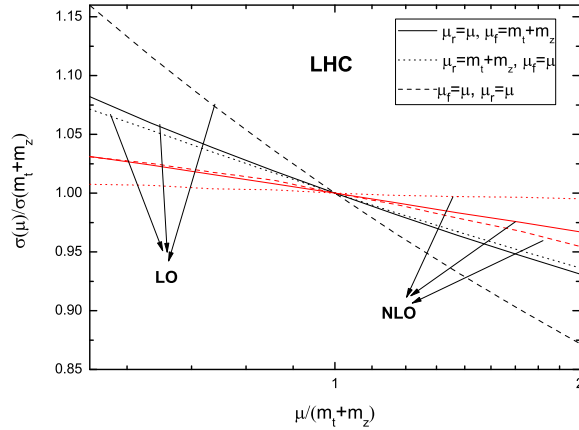


FIG. 11: Scale dependence of the total cross sections for the gu initial state subprocess at the LHC, the black lines represent the LO results, while the red ones represent the NLO results.

In Figs. 11 we show the scale dependence of the LO and NLO total cross section at LHC for three cases: (1) the renormalization scale dependence $\mu_r = \mu$, $\mu_f = m_t + m_Z$; (2) the factorization scale dependence $\mu_r = m_t + m_Z$, $\mu_f = \mu$; and (3) total scale dependence $\mu_r = \mu_f = \mu$. It can be seen that the NLO corrections reduce the scale dependence significantly for all three cases, which make the theoretical predictions more reliable.

VI. CONCLUSIONS

We have calculated the NLO QCD corrections to the tZ associated production via the tqZ and tqg FCNC couplings at hadron colliders, respectively, and we also consider the mixing effects of these two couplings. Our results show that, for the tuZ coupling the NLO corrections can enhance the total cross sections by about 60% and 42%, and for the tcZ coupling by about 51% and 43% at the Tevatron and LHC, respectively. The NLO corrections can enhance the total cross sections by about 27% and 42% for the tug and the tcg couplings, respectively, at the LHC. The mixing effects between the tqZ and tqg FCNC couplings for this process can be either large or small depending on the values of various anomalous couplings. If we set $\kappa_g/\Lambda = \kappa_z/\Lambda = 0.01\text{TeV}^{-1}$ and $|g_{gL}|^2 = |g_{gR}|^2 = \text{Re}(g_{gL}g_{ZL}^*) = \text{Re}(g_{gR}g_{ZR}^*) = 1$, the NLO corrections can enhance the total cross sections by about 28% for tuV couplings, and by 42% for tcV couplings at the LHC. Moreover, the

NLO corrections reduce the dependence of the total cross sections on the renormalization or factorization scale significantly.

Acknowledgments

This work was supported in part by National Nature Science Foundation of China, Under Grants No. 10975004, and No. 11021092.

APPENDIX

In this appendix we give the LO results of the tZ associated production induced by the tqg and tqZ FCNC couplings, and the definition of the A and B_{\pm} .

$$\begin{aligned}
\overline{|M^B|^2}_{gq}(s, t) = & \frac{16\pi^2\alpha\alpha_s}{27st^2\Lambda^2\sin(2\theta)^2(s-m_t^2)^2(t-m_t^2)^2m_z^2} \{ (9t^2g_{\text{ZL}}^2(s-m_t^2)^2(2m_t^8 - (3 \\
& m_z^2 + 4s + 2t)m_t^6 + (2m_z^4 - (2s+t)m_z^2 + 2(s^2 + 4ts + t^2))m_t^4 + (2 \\
& m_z^6 - 4tm_z^4 + (s^2 + 6ts + 5t^2)m_z^2 - 2t(3s^2 + 6ts + t^2))m_t^2 + t \\
& (-2m_z^6 + 2(s+t)m_z^4 - (s+t)^2m_z^2 + 4st(s+t)))\kappa_z^2m_z^2 + 9t^2 \\
& g_{\text{ZR}}^2(s-m_t^2)^2(2m_t^8 - (3m_z^2 + 4s + 2t)m_t^6 + (2m_z^4 - (2 \\
& s+t)m_z^2 + 2(s^2 + 4ts + t^2))m_t^4 + (2m_z^6 - 4tm_z^4 + (s^2 + 6ts + 5t^2) \\
& m_z^2 - 2t(3s^2 + 6ts + t^2))m_t^2 + t(-2m_z^6 + 2(s+t)m_z^4 - (s+t)^2m_z^2 + 4st \\
& (s+t)))\kappa_z^2m_z^2 + 6stg_{\text{gL}}g_{\text{ZL}}(s-m_t^2)(t-m_t^2)(-2(4\text{sw}^2 - 3)(3t-m_z^2)m_t^6 + 2(s \\
& (3 - 4\text{sw}^2)m_z^2 + t(s(16\text{sw}^2 - 9) + 4(4\text{sw}^2 - 3)t))m_t^4 + t(-8s^2\text{sw}^2 + 2(3 - 4\text{sw}^2) \\
& t^2 + (-8t\text{sw}^2 + s(16\text{sw}^2 - 9) + 6t)m_z^2 + 12s(1 - 2\text{sw}^2)t)m_t^2 + st^2(8s\text{sw}^2 + \\
& 8t\text{sw}^2 + (3 - 8\text{sw}^2)m_z^2 - 6t))\kappa_g\kappa_zm_z^2 + 6stg_{\text{gR}}g_{\text{ZR}}(s-m_t^2)(t-m_t^2) \\
& (8\text{sw}^2(m_z^2 - 3t)m_t^6 + (2t(16t\text{sw}^2 + s(16\text{sw}^2 - 3)) - 8s\text{sw}^2m_z^2)m_t^4 - t \\
& ((8\text{sw}^2 - 6)s^2 + 6(4\text{sw}^2 - 1)ts + 8\text{sw}^2t^2 + (8t\text{sw}^2 + s(3 - 16 \\
& \text{sw}^2))m_z^2)m_t^2 + st^2(8t\text{sw}^2 + (3 - 8\text{sw}^2)m_z^2 + s(8\text{sw}^2 - 6)))\kappa_g\kappa_zm_z^2 - s(t-m_t^2)^2 \\
& ((2(3 - 4\text{sw}^2)^2m_z^2(m_z^2 - t)m_t^8 + 2(3 - 4\text{sw}^2)^2m_z^2(t(s+2t) - 2(s+t)m_z^2)m_t^6 - \\
& 2(3 - 4\text{sw}^2)^2(s^2 + 4ts + t^2)m_z^2(t-m_z^2)m_t^4 + st(-4(3 - 4\text{sw}^2)^2 \\
& (s+t)m_z^4 + (2s^2(3 - 4\text{sw}^2)^2 + 6t^2(3 - 4\text{sw}^2)^2 + 3s(64 \\
& \text{sw}^4 - 64\text{sw}^2 + 15)t)m_z^2 - 9st^2)m_t^2 + s^2t^2(2(32 \\
& \text{sw}^4 - 24\text{sw}^2 + 9)m_z^4 - 2(32\text{sw}^4 - 24\text{sw}^2 + 9)(s+t)m_z^2 + 9s \\
& t))g_{\text{gL}}^2 + g_{\text{gR}}^2(32\text{sw}^4m_z^2(m_z^2 - t)m_t^8 + 32 \\
& \text{sw}^4m_z^2(t(s+2t) - 2(s+t)m_z^2)m_t^6 - 32\text{sw}^4(s^2 + 4ts + t^2) \\
& m_z^2(t-m_z^2)m_t^4 + st(-64\text{sw}^4(s+t)m_z^4 + (32s^2\text{sw}^4 + 96t^2 \\
& \text{sw}^4 + 3s(64\text{sw}^4 - 32\text{sw}^2 + 3)t)m_z^2 - 9st^2)m_t^2 + s^2t^2 \\
& (2(32\text{sw}^4 - 24\text{sw}^2 + 9)m_z^4 - 2(32\text{sw}^4 - 24\text{sw}^2 + 9) \\
& (s+t)m_z^2 + 9st)))\kappa_g^2\} \}, \tag{45}
\end{aligned}$$

$$A = \frac{8\ln\left(-\frac{\beta+1}{\beta-1}\right)}{\beta}, \quad (46)$$

$$B^+ = -2\text{Li2}\left(\frac{-\beta(m_t^2 - m_z^2 + s) + m_t^2 + m_z^2 - s - 2u}{2m_t^2 - 2u}\right) + 2\text{Li2}\left(\frac{\frac{m_t^2 + m_z^2 - s - 2u}{m_t^2 - m_z^2 + s} + \beta}{\beta - 1}\right) + \ln^2\left(-\frac{(\beta - 1)(m_t^2 - m_z^2 + s)}{2(m_t^2 - u)}\right) - \frac{1}{2}\ln^2\left(-\frac{\beta + 1}{\beta - 1}\right), \quad (47)$$

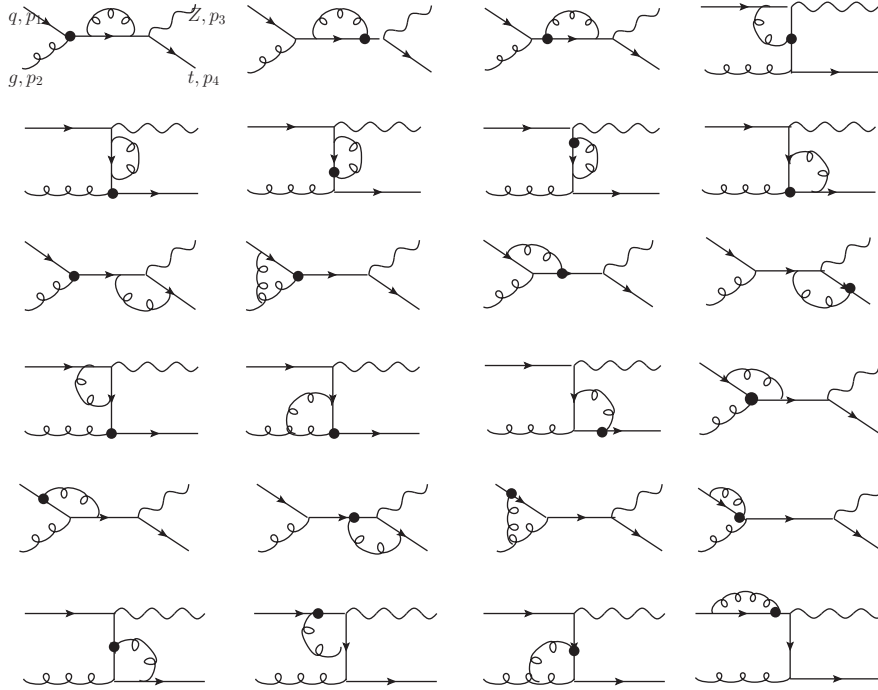
$$B^- = -2\text{Li2}\left(\frac{-(\beta + 1)m_t^2 + (\beta - 1)m_z^2 - s\beta + s + 2u}{2(m_z^2 - s - u)}\right) + 2\text{Li2}\left(\frac{\frac{-m_t^2 - m_z^2 + s + 2u}{m_t^2 - m_z^2 + s} + \beta}{\beta - 1}\right) + \ln^2\left(\frac{(\beta - 1)(m_t^2 - m_z^2 + s)}{2(m_z^2 - s - u)}\right) - \frac{1}{2}\ln^2\left(-\frac{\beta + 1}{\beta - 1}\right), \quad (48)$$

where $\beta = \sqrt{1 - \frac{4sm_t^2}{(m_t^2 - m_z^2 + s)^2}}$.

-
- [1] S. L. Glashow, J. Iliopoulos and L. Maiani, Phys. Rev. D **2** (1970) 1285.
- [2] J. A. Aguilar-Saavedra, Acta Phys. Polon. B **35** (2004) 2695.
- [3] F. Larios, R. Martinez and M. A. Perez, Int. J. Mod. Phys. A **21**, 3473 (2006) [arXiv:hep-ph/0605003].
- [4] T. P. Cheng and M. Sher, Phys. Rev. D **35** (1987) 3484; M. E. Luke and M. J. Savage, Phys. Lett. B **307** (1993) 387; D. Atwood, L. Reina and A. Soni, Phys. Rev. D **55** (1997) 3156; S. Bejar, J. Guasch and J. Sola, Nucl. Phys. B **600** (2001) 21.
- [5] C. S. Li, R. J. Oakes and J. M. Yang, Phys. Rev. D **49** (1994) 293 [Erratum-ibid. D **56** (1997) 3156]; J. L. Lopez, D. V. Nanopoulos and R. Rangarajan, Phys. Rev. D **56** (1997) 3100; G. M. de Divitiis, R. Petronzio and L. Silvestrini, Nucl. Phys. B **504** (1997) 45; J. M. Yang, B. L. Young and X. Zhang, Phys. Rev. D **58** (1998) 055001; J. Guasch and J. Sola, Nucl. Phys. B **562** (1999) 3; G. Eilam, A. Geminien, T. Han, J. M. Yang and X. Zhang, Phys. Lett. B **510** (2001) 227; J. j. Cao, Z. h. Xiong and J. M. Yang, Phys. Rev. Lett. **88** (2002) 111802; J. J. Liu, C. S. Li, L. L. Yang and L. G. Jin, Phys. Lett. B **599** (2004) 92, M. Herquet, R. Kneijens and E. Laenen, Phys. Lett. B **693** (2010) 591 [arXiv:1005.2900 [hep-ph]].
- [6] H. Davoudiasl and T. G. Rizzo, Phys. Lett. B **512** (2001) 100; P. M. Aquino, G. Burdman and O. J. P. Eboli, Phys. Rev. Lett. **98** (2007) 131601; S. Casagrande, F. Goertz, U. Haisch,

- M. Neubert and T. Pfoh, JHEP **0810** (2008) 094; J. Gao, C. S. Li, X. Gao and Z. Li, Phys. Rev. D **78** (2008) 096005.
- [7] W. Buchmuller and D. Wyler, Nucl. Phys. B **268** (1986) 621.
- [8] M. Beneke *et al.*, arXiv:hep-ph/0003033.
- [9] T. Aaltonen *et al.* [CDF Collaboration], Phys. Rev. Lett. **101** (2008) 192002 [arXiv:0805.2109 [hep-ex]].
- [10] J. J. Zhang, C. S. Li, J. Gao, H. Zhang, Z. Li, C. P. Yuan and T. C. Yuan, Phys. Rev. Lett. **102** (2009) 072001.
- [11] J. J. Zhang, C. S. Li, J. Gao, H. X. Zhu, C. P. Yuan and T. C. Yuan, Phys. Rev. D **82**, 073005 (2010) [arXiv:1004.0898 [hep-ph]].
- [12] J. Drobnak, S. Fajfer and J. F. Kamenik, Phys. Rev. Lett. **104**, 252001 (2010) [arXiv:1004.0620 [hep-ph]].
- [13] P. J. Fox, Z. Ligeti, M. Papucci, G. Perez and M. D. Schwartz, Phys. Rev. D **78**, 054008 (2008) [arXiv:0704.1482 [hep-ph]].
- [14] V. M. Abazov *et al.* [D0 Collaboration], arXiv:1103.4574 [hep-ex].
- [15] V. M. Abazov *et al.* [D0 Collaboration], Phys. Lett. B **693**, 81 (2010).
- [16] T. Aaltonen *et al.* [CDF Collaboration], Phys. Rev. Lett. **102**, 151801 (2009).
- [17] J. J. Liu, C. S. Li, L. L. Yang and L. G. Jin, Phys. Rev. D **72**, 074018 (2005).
- [18] J. Gao, C. S. Li, J. J. Zhang and H. X. Zhu, Phys. Rev. D **80**, 114017 (2009).
- [19] L. L. Yang, C. S. Li, Y. Gao and J. J. Liu, Phys. Rev. D **73**, 074017 (2006).
- [20] J. A. Aguilar-Saavedra, Acta Phys. Polon. B **35**, 2695 (2004); J. A. Aguilar-Saavedra, Nucl. Phys. B **837**, 122 (2010);
- [21] N. Kidonakis and A. Belyaev, JHEP **0312**, 004 (2003).
- [22] T. Hahn, Comput. Phys. Commun. **140**, 418 (2001) [arXiv:hep-ph/0012260].
- [23] T. Hahn, PoS A **CAT2010**, 078 (2010) [arXiv:1006.2231 [hep-ph]].
- [24] G. 't Hooft and M. J. G. Veltman, Nucl. Phys. B **44** 189 (1972).
- [25] B. W. Harris and J. F. Owens, Phys. Rev. D **65** 094032 (2002).
- [26] A. Denner, Fortsch. Phys. **41** 307 (1993).
- [27] R. K. Ellis and G. Zanderighi, JHEP **0802** 002 (2008).
- [28] S. Frixione, E. Laenen, P. Motylinski, B. R. Webber and C. D. White, JHEP **0807**, 029 (2008) [arXiv:0805.3067 [hep-ph]].

- [29] T. M. P. Tait, Phys. Rev. D **61**, 034001 (2000) [arXiv:hep-ph/9909352].
- [30] J. C. Collins, D. E. Soper and G. Sterman, Nucl. Phys. **B 261**, 104 (1985).
- [31] G. T. Bodwin, Phys. Rev. **D 31**, 2616 (1985);
- [32] G. Altarelli, R. K. Ellis, and G. Martinelli, Nucl. Phys. **B 157**, 461 (1979)
- [33] J. C. Collins, D. E. Soper and G. Sterman, Adv. Ser. Direct. High Energy Physics. 5, 1 (1988)
- [34] K. Nakamura *et al.* [Particle Data Group], J. Phys. G **37**, 075021 (2010).
- [35] C. Amsler *et al.* [Particle Data Group], Phys. Lett. B **667** (2008) 1.
- [36] J. Pumplin, D. R. Stump, J. Huston, H. L. Lai, P. M. Nadolsky and W. K. Tung, JHEP **0207** (2002) 012.



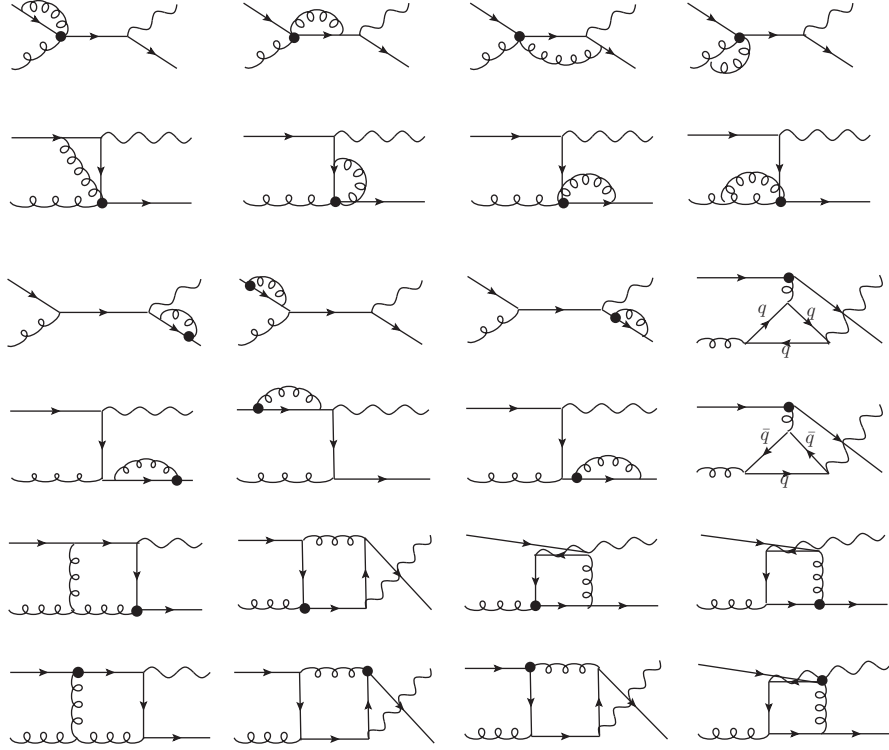
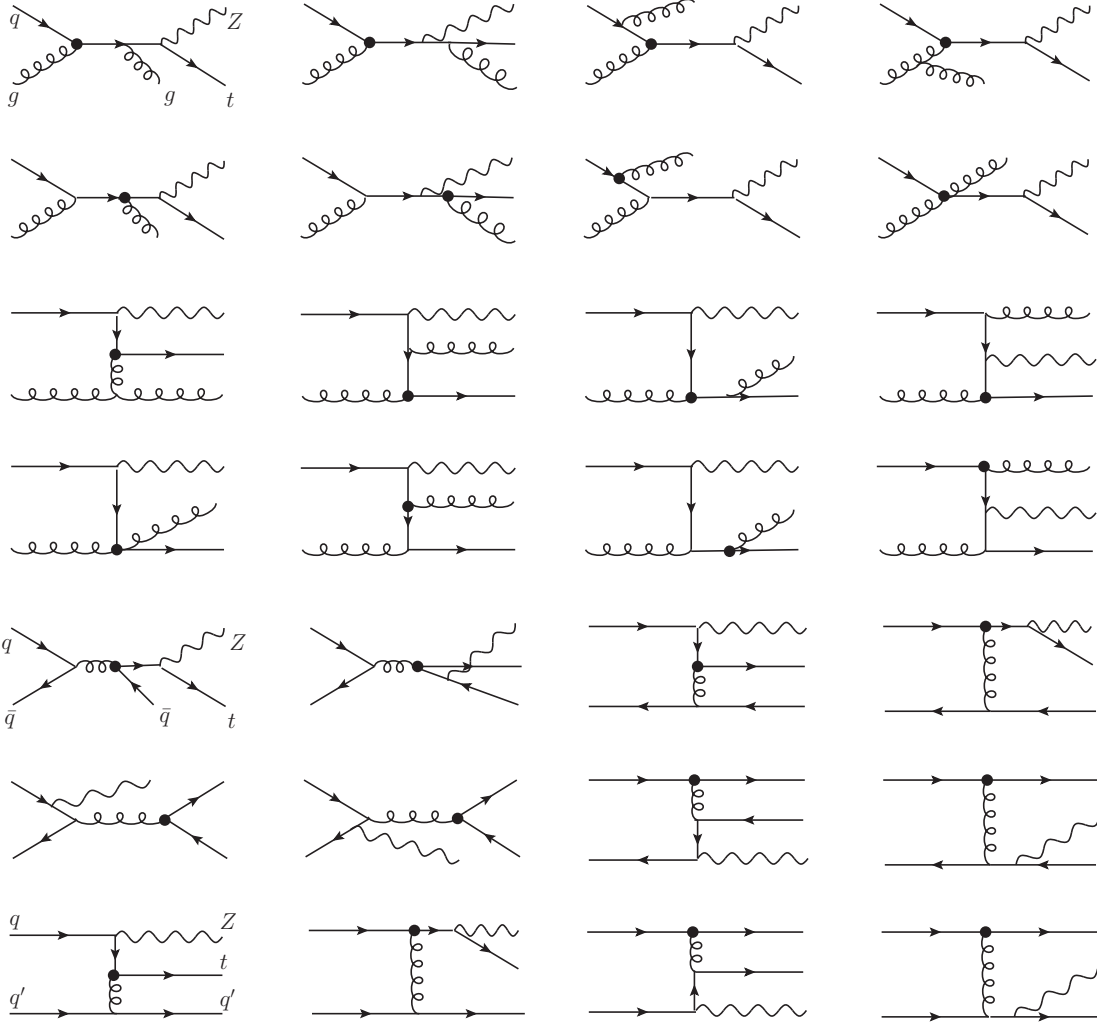


FIG. 12: 1-loop Feynman diagrams for the single top quark production via the FCNC couplings with operator mixing.



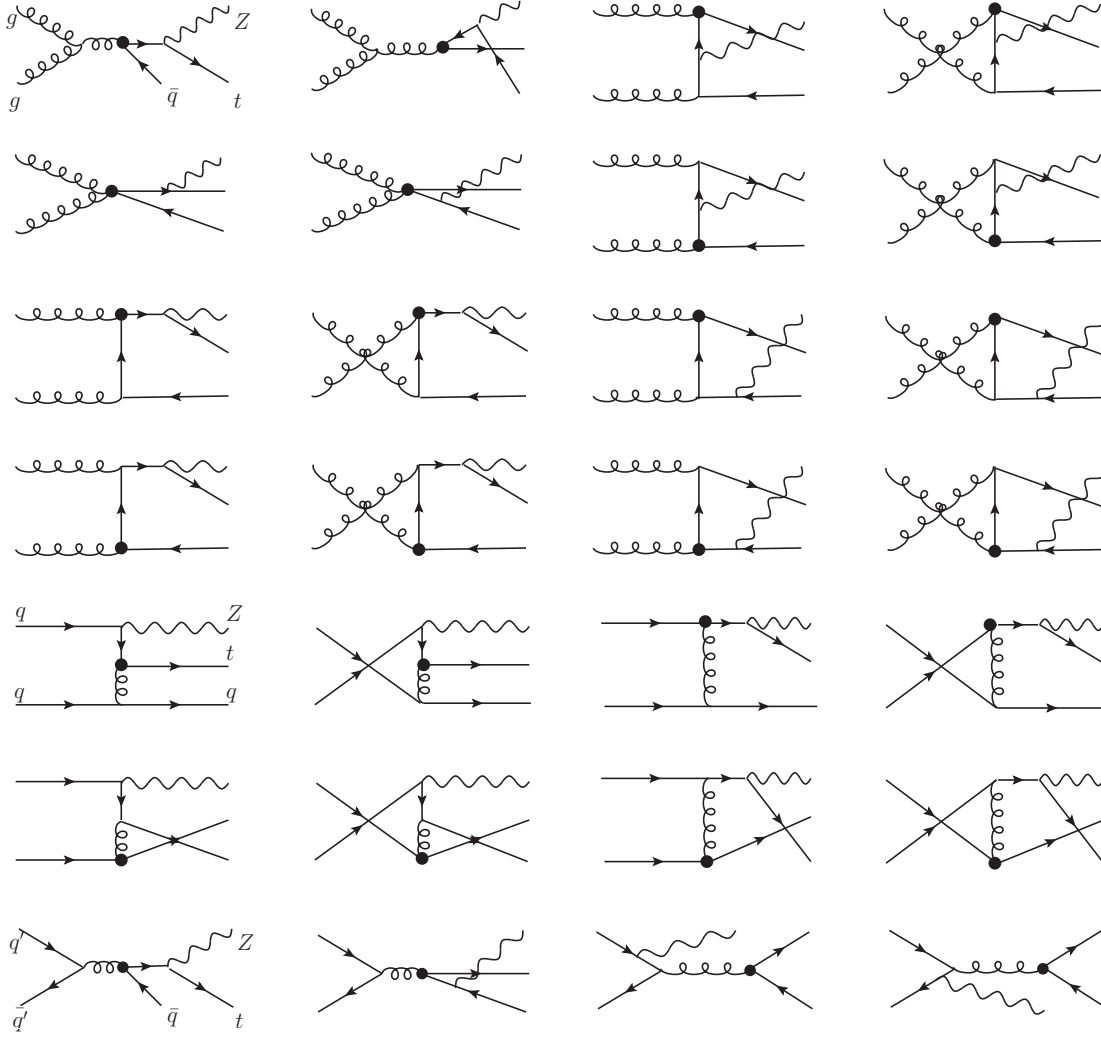


FIG. 13: Feynman diagrams of the real corrections for the single top quark production via the FCNC couplings with operator mixing.